Evolution of the Magnetic Structure of Hexagonal HoMnO₃ from Neutron Powder Diffraction Data

A. Muñoz,*,† J. A. Alonso,‡ M. J. Martínez-Lope,‡ M. T. Casáis,‡ J. L. Martínez,‡ and M. T. Fernández-Díaz§

Departamento de Física, EPS, Universidad Carlos III, Avenida de la Universidad 30, Leganés E-28911 Madrid, Spain, Instituto de Ciencia de Materiales de Madrid, Consejo Superior de Investigaciones Científicas, Cantoblanco, E-28049 Madrid, Spain, and Institut Laue-Langevin, BP 156X, 38042 Grenoble Cedex 9, France

Hexagonal, nonperovskite HoMnO₃ oxide, containing a triangular arrangement of Mn³⁺ cations, has been prepared in polycrystalline form by the thermal decomposition of metal citrates. The crystal structure has been refined from neutron powder diffraction data. Magnetic and specific-heat measurements anticipate a complex phase diagram: HoMnO₃ becomes magnetically ordered at $T_N \approx 72$ K, and another two magnetic transitions take place at lower temperatures. Neutron powder diffraction measurements demonstrate that, below the ordering temperature, the moments of the Mn³⁺ cations adopt a triangular spin arrangement, the magnetic moments lying in the basal plane and parallel to the [100] axis. At $T = 44.6$ K, the moments suddenly reorientate within the basal plane and become aligned perpendicularly to the initial direction. Below $T = 25.4$ K, an ordered magnetic moment is observed on the Ho atoms at the 4b sites of the crystal structure, whereas those of the 4a site remain in a paramagnetic state. The Ho atoms adopt an antiferromagnetic structure with the moments parallel to the c axis. At 1.7 K, the ordered moment on the Mn³⁺ cations is 3.05(2) μ_B, and that on the Ho³⁺ cations is 2.97(3) MB.

1. Introduction

The prospect of important technological applications of the compounds exhibiting colossal magnetoresistance (CMR)[1] has originated numerous investigations of the perovskite manganites $R_{1-x}A_xMnO_3$ (R = lanthanides; A = Ca, Sr, Ba) in the past several years.[2-7] The chemical doping of RMnO₃ with divalent ions makes possible the introduction of electronic holes in the Mn–O bands, i.e., the presence of both Mn³⁺ and Mn⁴⁺ ions in these compounds. The electronic transfer between neighboring Mn³⁺ and Mn⁴⁺ cations via the so-called double-exchange mechanism[8-10] qualitatively accounts for the simultaneous metallic state and ferromagnetism observed below T_C. However, recent experiments and theoretical studies[11,12] have indicated that additional factors such as Jahn–Teller distortion of the MnO₆ octahedra and electron–phonon coupling are also important ingredients in explaining the physical properties of these systems.

The revival of interest in CMR perovskite manganites has made necessary the investigation of more basic aspects of undoped RMnO₃ compounds, in particular, their peculiar magnetic structure and orbital ordering.[13-15] LaMnO₃, together with the other RMnO₃ manganites for rare-earth cations up to Dy, crystallize in an orthorhombic structure (space group *Pnma*).[16,17] For rare earth cations with smaller ionic radii (those from Ho to Lu, Y, and Sc), a second crystallographic nonperovskite hexagonal structure strongly competes in stability. These hexagonal manganites (space group $P6_3cm$)[18] can be transformed into the orthorhombic perovskite phases by annealing under high pressure.[19,20] The early studies

* Corresponding author. Electronic address: amunoz@fis.uc3m.es.
† Universidad Carlos III.
‡ Consejo Superior de Investigaciones Científicas.
§ Institut Laue-Langevin.

(1) Jin, S.; Tiefel, H. T.; McCormack, M.; Fastnacht, A. *Science* **1994**, *264*, 413.
(2) Kuster, R. M.; Singeton, J.; Keon, D. A.; Greedy, R. M.; Hayes, W. *Physica B* **1989**, *155*, 362.
(3) Hemmolt, R. V.; Wecker, J.; Holzapfel, B.; Schultz, L.; Samwer, K. *Phys. Rev. Lett.* **1993**, *71*, 2331.
(4) Chahara, K.; Ohno, T.; Kasai, M.; Jozono, Y. *Appl. Phys. Lett.* **1993**, *63*, 1190.
(5) McCormack, M.; Jin, S.; Tiefel, T. H.; Fleming, R. M.; Phillips, J. M.; Ramesh, R. *Appl. Phys. Lett.* **1994**, *64*, 3045.
(6) Maignan, A.; Simon, Ch.; Caignaert, V.; Raveau, B. *Solid State Commun.* **1995**, *96*, 623.
(7) Urushibara, A.; Moritomo, Y.; Arima, T.; Asamitsu, A.; Kido, G.; Tokura, Y. *Phys. Rev. B* **1995**, *51*, 14103.
(8) Zener, C. *Phys. Rev.* **1951**, *82*, 403.
(9) Anderson, P. W.; Hasegawa, H. *Phys. Rev.* **1955**, *100*, 675.
(10) De Gennes, P. G. *Phys. Rev.* **1960**, *118*, 141.
(11) Tokura, Y., Ed. *Colossal Magnetoresistance Oxides*; Monographs in Condensed Matter Science; Gordon & Breach: Langhorne, PA, 1999.
(12) Ramirez, A. P. *J. Phys. Condens. Matter* **1997**, *9*, 8171.
(13) Saitoh, T.; Boucquet, A. E.; Mizokawa, T.; Namatame, H.; Fujimori, A.; Abbate, M.; Takeda, Y.; Takano, M. *Phys. Rev. B* **1995**, *51*, 13942.
(14) Solovyev, I.; Hamada, N.; Terakura, K. *Phys. Rev. Lett.* **1996**, *76*, 4825.
(15) Moussa, F.; Hennion, M.; Rodríguez-Carvajal, J.; Moudden, H. *Phys. Rev. B* **1996**, *54*, 15149.
(16) Bertaut, E. F.; Forrat, F. *J. Phys.* **1956**, *17*, 129.
(17) Gilleo, M. A. *Acta Crystallogr.* **1957**, *10*, 161.
(18) Yakel, H.; Koehler, W. C.; Bertaut, E. F.; Forrat, F. *Acta Crystallogr.* **1963**, *16*, 957.
(19) Waintal, A.; Chenavas, J. *C. R. Hebd. Séances Acad. Sci.* 1967, *264B*, 168; *Mater. Res. Bull.* **1967**, *2*, 819.

carried out on hexagonal manganites[21,22] showed that they exhibit an antiferromagnetic (AFM) ordering with a T_N ranging from 70 to 130 K. Furthermore, they undergo a ferroelectric transition at high temperatures (600–900 K);[23,24] therefore, unlike orthorhombic perovskites, at low temperature, there is a coexistence of magnetic ordering and ferroelectricity.

In the crystal structure of hexagonal $RMnO_3$, there are six molecules per unit cell, with the Mn atoms placed along the [100] axis in the $z = 0$ and $z = 1/2$ layers. According to neutron diffraction studies,[21,22] the magnetic moments of the Mn ions lie in the basal ab plane and adopt a triangular magnetic structure, although there exists an ambiguity about whether the coupling between the $z = 0$ and $z = 1/2$ layers is ferromagnetic (FM) or AFM. This frustrated-AFM structure seems to be related to the presence of both FM and AFM interactions among the Mn ions. The magnetic moments are usually directed along some of the [100] directions, although in some compounds, such as $ScMnO_3$,[25] the moments can undergo a reorientation within the basal plane.

Recently, a nonlinear optical spectroscopy method,[26] second harmonic generation, has been applied to clarify the magnetic structure of the hexagonal $RMnO_3$ manganites. This technique has enabled the determination of the tensor components of the magnetic susceptibility and the magnetic space group. Such experiments[27] suggest that the coupling between the $z = 0$ and $z = 1/2$ layers is FM in all of the hexagonal $RMnO_3$ manganites. However, in the case of $ScMnO_3$, the presence of weak ferromagnetism[25,28,29] seems not to be compatible with a ferromagnetic coupling between layers.[29,30]

In this paper, the magnetic structure of the hexagonal $HoMnO_3$ is revisited, and a detailed study of its thermal evolution down to 1.7 K is presented, describing a moment reorientation of the Mn spins. The possible ordering of the Ho ions is also analyzed. Neutron diffraction data are complemented by magnetization and specific-heat measurements. The refinement of the crystallographic structure, from high-resolution neutron powder diffraction, is also reported.

2. Experimental Section

2.1. Sample Preparation. Hexagonal $HoMnO_3$ was prepared as a polycrystalline powder by a liquid-mix technique. Stoichiometric amounts of analytical-grade Ho_2O_3 and $MnCO_3$ were dissolved in citric acid by adding several droplets of concentrated HNO_3 to favor the solution of Ho_2O_3; the citrate + nitrate solution was slowly evaporated, leading to an organic resin that was first dried at 120 °C and then decomposed by heating at temperatures up to 800 °C in air. The precursor powder was finally heated at 1100 °C in air for 12 h, thus yielding a well-crystallized monophase powder. The final treatment at relatively high temperatures was necessary to avoid the formation of the competitive orthorhombic $HoMnO_3$ perovskite, which is stabilized at lower temperatures. [31]

2.2. Characterization. The product was initially characterized by laboratory XRD (Cu Kα, λ = 1.5406 Å) for phase identification and assessment of phase purity. Scanning electron microscopy (SEM) micrographs were recorded with a Philips XL30 microscope at an accelerating voltage of 10 kV and magnification values up to 5.000×. The $HoMnO_3$ SEM images were taken on compacted pellets that were sintered under the same synthetic conditions (1100 °C, air) as the raw powder.

2.3. Macroscopic Measurements. Magnetic measurements were carried out in a commercial SQUID magnetometer. The dc susceptibility was measured under both zero-field-cooled (ZFC) and field-cooled (FC) conditions with a magnetic field of 1 kOe and for temperatures ranging from 9 to 300 K. The ac susceptibility was obtained in an oscillating magnetic field of 1 and 10 kHz in the temperature interval $2 < T < 240$ K. Isothermal magnetization curves were acquired at $T = 1.8$ K for fields up to 90 kOe and at 25 and 100 K for fields up to 50 kOe. The specific heat was measured in a semi-adiabatic He calorimeter by the heat-pulsed method, with the temperature varied from 2 to 110 K and under magnetic fields of 0, 5, 30, and 90 kOe.

2.4. Neutron Data. The neutron diffraction experiments were carried out at the Institute Laue-Langevin in Grenoble (France). A high-resolution neutron powder diffraction (NPD) pattern collected at the D2B diffractometer at room temperature with λ = 1.594 Å was used for refinement of the crystallographic structure. For the analysis of the thermal evolution of the magnetic structure, a set of NPD patterns was collected at the D20 diffractometer, at temperatures ranging from 1.7 to 126 K and with a wavelength of λ = 2.42 Å. In both cases, a 4-g powder sample was contained in a vanadium can. The refinement of both the crystallographic and the magnetic structures was done with the program FULLPROF[32] using the Rietveld method.[33] The magnetic form factors used were determined with the coefficients taken from the International Tables.[34] For Mn^{3+} ions, the spin-only $\langle j_0 \rangle$ coefficients were used; the dipolar approximation was considered for Ho^{3+} ions by using the $\langle j_0 \rangle$ and $\langle j_2 \rangle$ coefficients.

3. Results from Macroscopic Measurements

$HoMnO_3$ was obtained as a black, well-crystallized powder. The laboratory XRD diagram is shown in Figure 1. The pattern shows sharp, well-defined reflections. No impurity phases were detected from either the XRD or the NPD data. Two micrographs (Figure 2) of as-grown $HoMnO_3$ illustrate the high homogeneity of this material. Figure 2 shows the presence of porosity, probably formed during the elimination of organic materials. $HoMnO_3$ microcrystals are well-sintered, forming intercrossed chainlike structures. The size of the individual microcrystals is in the range of 1–2 μm.

3.1. Magnetic Measurements. The thermal evolution of the dc magnetic susceptibility is shown in Figure 3. No anomalies that could indicate the onset of a

(20) Wood, W. E.; Austin, A. E.; Collins, E. W.; Brog, K. C. *J. Phys. Chem. Solids* **1973**, *34*, 859.

(21) Bertaut, E. F.; Mercier, M.; Pauthenet, R. *J. Phys.* **1964**, *25*, 550.

(22) Koehler, W. C.; Yakel, H. L.; Wollan, E. O.; Cable, J. W. *Phys. Lett.* **1964**, *9*, 93.

(23) Smolenskii, G. A.; Chupis, I. E. *Sov. Phys.-Usp.* **1982**, *25*, 475.

(24) Ismaelzade, I. G.; Kizhaev, S. A. *Sov. Phys. Solid State* **1965**, *7*, 236.

(25) Bieringer, M.; Greedan, J. E. *J. Solid State Chem.* **1999**, *143*, 132.

(26) Fiebig, M.; Fröhlich, D.; Sluyterman, G.; Pisarev, R. V. *Phys. Rev. Lett.* **1994**, *73*, 2127.

(27) Fiebig, M.; Fröhlich, D.; Kohn, K.; Leute, St.; Lottermoser, Th.; Pavlov, V. V.; Pisarev, R. V. *Phys. Rev. Lett.* **2000**, *84*, 5620.

(28) Xu, H. W.; Iwasaki, J.; Shimizu, T.; Satoh, H.; Kamegashira, N. *J. Alloys Compd.* **1995**, *221*, 274.

(29) Muñoz, A.; Alonso, J. A.; Martínez-Lope, M. J.; Casais, M. T.; Martínez, J. L.; Fernández-Díaz, M. T. *Phys. Rev. B* **2000**, *62*, 9498.
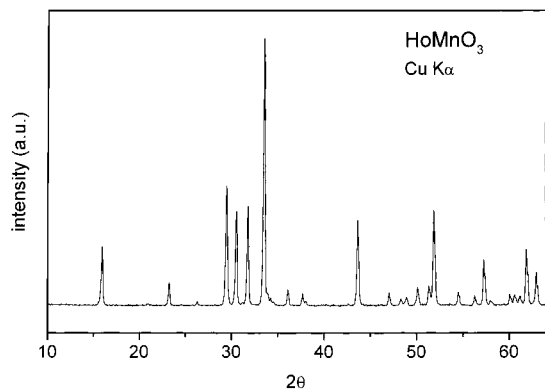
(30) Nedlin, G. M. *Sov. Phys. Solid State* **1965**, *6*, 2156.

(31) Alonso, J. A.; Martínez-Lope, M. J.; Casais, M. T.; Fernández-Díaz, M. T. *Inorg. Chem.* **2000**, *39*, 917.
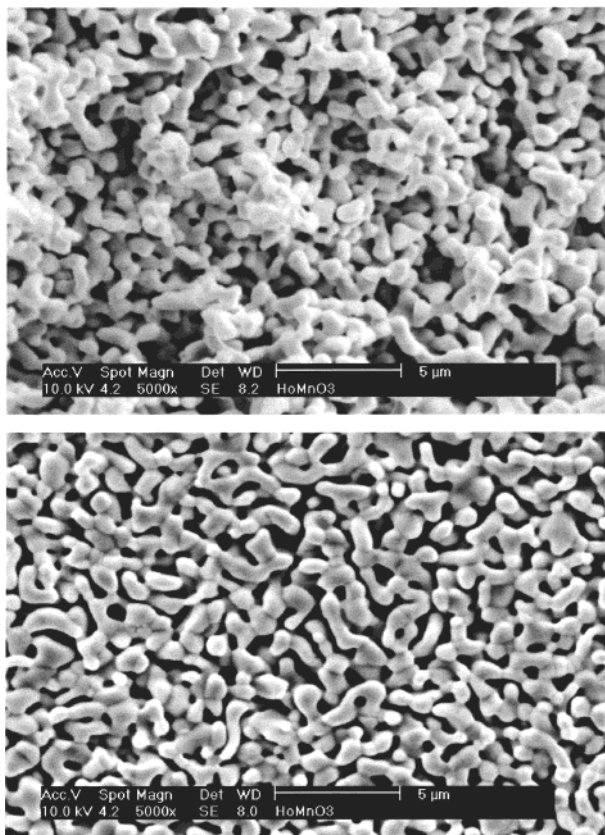
(32) Rodríguez-Carvajal, J. *Physica B* **1993**, *192*, 55.

(33) Rietveld, H. M. *J. Crystallogr.* **1969**, *2*, 65.

(34) Wilson, A. J. C., Ed. *International Tables for Crystallography*; Kluwer Academic Publishers: Norwell, MA, 1992; Vol. C, p 391.
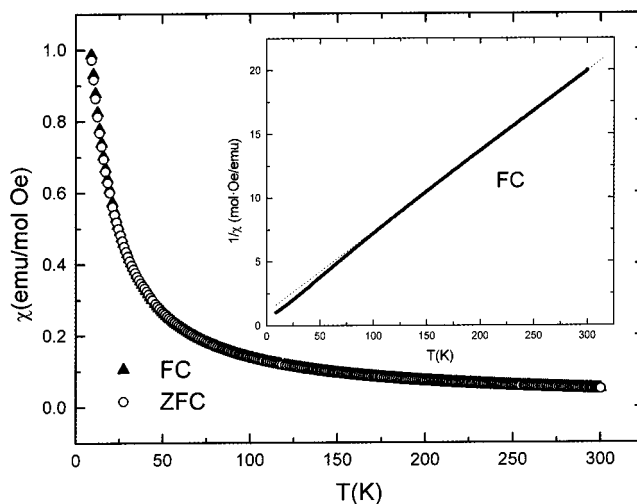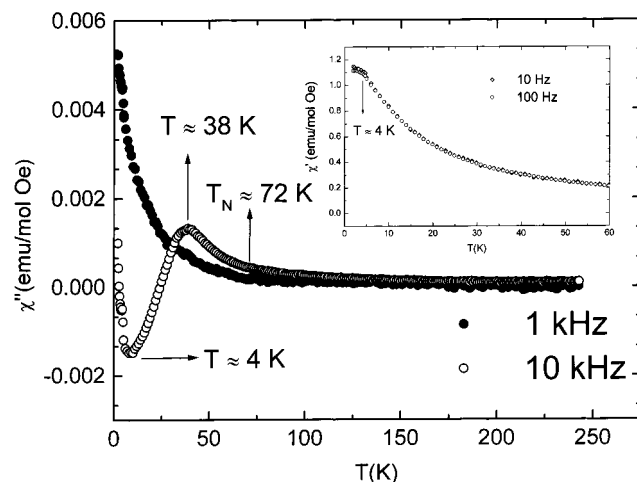
Figure 1. XRD pattern of hexagonal HoMnO₃.

Figure 2. Scanning electron micrographs of a sintered pellet of HoMnO₃ taken at a magnification of 5.000×.

Figure 3. Thermal evolution of the zero-field-cooled (ZFC) and the field-cooled (FC) dc susceptibility under a magnetic field of 1 kOe. Inset: Inverse of the magnetic susceptibility.


Figure 4. Thermal evolution of the imaginary part of the ac susceptibility under a 1 and 10 kHz oscillating magnetic field. Inset: Real part of the ac susceptibility.

magnetic ordering (as pointed out by Pauthenet et al.[35]) are observed in the curve. It is very possible that the magnetic transition is masked by the high paramagnetic susceptibility associated with the Ho³⁺ ions. On the other hand, at low temperature, there is no difference between the zero-field-cooled and the field-cooled susceptibility measurements, which implies the absence of weak ferromagnetism, in contrast with the observations for ScMnO₃.[29] Above 125 K, the susceptibility follows a Curie–Weiss law behavior characterized by a paramagnetic temperature $\theta_P = -17$ K and an effective paramagnetic moment $\mu_{eff} = 11.3\ \mu_B$. This value is very close to the theoretical one calculated as $\mu_{eff} = [\mu_{eff}(Mn)^2 + \mu_{eff}(Ho)^2]^{1/2} = 11.50\ \mu_B$, where the values 4.9 μ_B for Mn³⁺ ion (spin-only) and 10.4 μ_B ($J = 8$) for Ho³⁺ have been considered. The ac susceptibility measurements are

presented in Figure 4. In the imaginary part of the susceptibility, a different behavior is observed at 10 kHz below 72 K, which is related to the onset of the magnetic ordering of the Mn sublattice. After exhibiting a maximum at around 38 K, the susceptibility decreases, experiences a minimum value at around 4 K, and then increases again. The minimum is related to the temperature at which the real part of the susceptibility seems to reach saturation. As will be shown from the neutron diffraction data, the anomaly observed at 38 K is due to a magnetic transition involving a reorientation of the Mn magnetic moments, and the transition at around 4 K is related to the onset of the magnetic ordering of the Ho³⁺ ions.

The isothermal magnetization curves are presented in Figure 5. At $T = 1.8$ K, the magnetization shows a linear behavior up to 20 kOe, reaching a value of 7.8 μ_B for $H = 90$ kOe, although saturation is not achieved. At $T = 25$ K, the magnetization is linear up to 30 kOe, probably because of the high contribution from the Ho³⁺ ions, which are not ordered at this temperature.

3.2. Specific-Heat Measurements. The evolution of the specific heat with temperature is given in Figure 6

(35) Pauthenet, R.; Veyret, C. *J. Phys.* **1970**, *31*, 65.
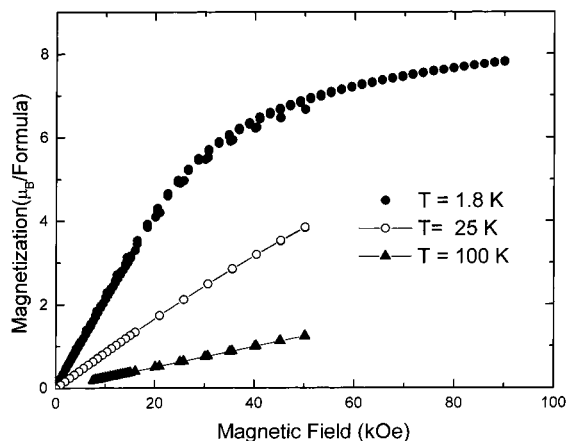
Figure 5. Isothermal magnetization curves.
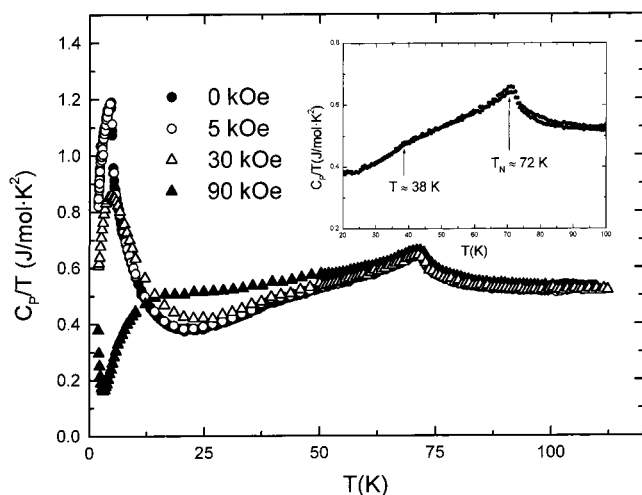
Figure 6. Specific-heat measurements under different magnetic fields. Inset: Specific heat under zero magnetic field for $20 < T < 100$ K.

as C_P/T versus temperature. In the zero-magnetic-field curve, a sharp anomaly is observed at $T_N \approx 72$ K, indicating the onset of a magnetic ordering. A small shoulder is observed at around 38 K (see inset of Figure 6), in good agreement with the observations of the ac susceptibility. Below 25 K, the specific heat undergoes an increase with a maximum at $T \approx 4$ K, again in good agreement with the magnetic transition detected in the ac susceptibility curve. The nonmagnetic contribution to the specific heat was calculated by considering three Einstein oscillators at high temperature and a linear behavior at low temperature. The change in entropy at the transition $T_N \approx 72$ K, calculated as $\Delta S = \int (C_{mag}/T)\, dT$, is 1.30 J/mol K, which is only 9.7% of $R \ln 5$, the entropy corresponding to the Mn^{3+} ion with $S = 2$. In the temperature range 30–60 K, the curve can be adjusted by $C_V = \gamma T + \beta T^3$, representing the linear term to the electron contribution. It results in $\gamma = 0.386$ J/(mol K²), and $\beta = 5 \times 10^{-5}$ J/(mol K).[4] The Debye temperature, calculated from the β parameter, is $\Theta_D = 584$ K, quite similar to the corresponding value of the isostructural $ScMnO_3$, 615 K.[29] Whereas the anomaly at $T = 72$ K is not affected by the magnetic field, the one observed at $T = 4$ K is shifted to lower temperature as the field increases. At the maximum field of 90 kOe, this anomaly is shifted below 2 K. The third maximum present at around 38 K is unchanged under a 5-kOe

magnetic field, but its presence is unclear under 30 and 90 kOe.

4. Results from Powder Neutron Diffraction Experiments

4.1. Crystal Structure Refinement. The crystal structure was refined from the high-resolution NPD data. All of the Bragg reflections were indexed within the hexagonal space group $P6_3cm$ with the unit-cell parameters $a = 6.1413(1)$ Å and $c = 11.4122(3)$ Å. The most important crystallographic parameters determined in the fitting and the corresponding discrepancy factors are reported in Table 1. Some selected atomic distances and bond angles are contained in Table 2. The good agreement between the observed and calculated patterns is illustrated in Figure 7. In each unit cell, there are six formula units. As shown in Figure 8, each Mn ion is surrounded by five oxygen atoms as nearest neighbors, forming a MnO_5 bipyramid with a triangular base of nonequivalent O3 and O4 ($\times 2$) oxygens, whereas the O1 and O2 atoms are at the apexes. The structure consists of layers of corner-sharing MnO_5 bipyramids separated along the c direction by Ho^{3+} layers. Mn−O1 and Mn−O2 are declined with respect to the c direction by 3.27° and 6.29°, respectively. The Ho atoms occupy two crystallographic independent sites, each of them showing a 7-fold coordination to oxygens and forming monocapped octahedra.

4.2. Magnetic Structure Resolution. The study of the thermal evolution of the magnetic structure of hexagonal $HoMnO_3$ has been carried out by using a set of NPD patterns acquired below 126 K with a wavelength of $\lambda = 2.42$ Å. The thermal evolution of the diffraction diagrams is shown in Figure 9. As the temperature is decreased below $T = 78.5$ K, some Bragg reflections forbidden by the $P6_3cm$ space-group symmetry, such as (101) and (201), start to be observed (see Figure 10). Simultaneously, the intensities of other permitted reflections, such as (102) and (104), gradually increase (see Figure 11). This indicates the onset of a magnetic ordering. At lower temperatures, new changes appear in the NPD patterns; in particular, below $T = 44.6$ K, the intensities of some reflections such as (101) and (201) dramatically decrease, and the peaks then disappear (see Figure 10). On the contrary, other reflections undergo an important increase in their intensity; furthermore, some reflections such as (100), (202) + (113), and (211) start to present a magnetic contribution (see Figure 12). This reveals the transition to another magnetic spin arrangement. Finally, as the temperature is decreased below 15.5 K, the integrated intensity of those magnetic peaks with l odd suddenly rise, this increment being especially important for the reflections (101), (201), and (211) (see Figures 10–12). In all cases, the magnetic peaks appear on permitted Bragg positions; hence, the different magnetic structures are characterized by the propagation vector **k** = 0.

The possible magnetic structures compatible with the crystal symmetry are obtained by the theory of group representation analysis described by Bertaut.[36] As the
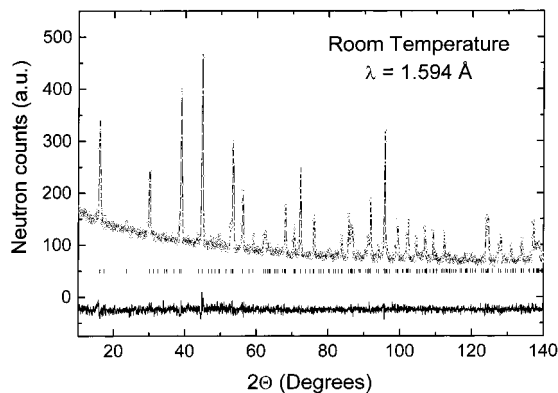
(36) Bertaut, E. F. *Magnetism*; Rado, G. T., Shul, H., Eds.; Academic Press: New York, 1963; Vol. III, Chapter 4, p 149.

Table 1. Lattice Parameters, Atomic Positions, and Discrepancy Factors Corresponding to the Fitting of the Crystallographic Structure of HoMnO₃

atoms		x	y	z	B (Å²)
Ho(1)	2a	0	0	0.2731(16)	0.18(5)
Ho(2)	4b	$1/3$	$2/3$	0.2306(12)	0.18(5)
Mn	6c	0.3224(32)	0	0	0.18(5)
O(1)	6c	0.3054(13)	0	0.1600(13)	0.52(5)
O(2)	6c	0.6433(12)	0	0.3326(13)	0.52(5)
O(3)	4b	0	0	0.4763(23)	0.63(6)
O(4)	2a	$1/3$	$2/3$	0.0170(15)	0.63(6)
unit cell		$a = 6.1413(1)$ Å	$c = 11.4122(3)$ Å	$V = 372.76(1)$ Å³	
discrepancy factors		$R_p = 3.7\%$	$R_{wp} = 4.7\%$	$R_{Brag} = 4.4\%$	$\chi^2 = 1.1$

Table 2. Selected Bond Lengths and Bond Angles

bond lengths (Å)		bond angles (°)	
Mn−O1	1.828(14)	O1−Mn−O2	176.9(9)
Mn−O2	1.922(15)	O1−Mn−O3	94.5(9)
Mn−O3	1.997(16)	O4−Mn−O4	116.0(3)
Mn−O4 (x2)	2.091(8)	O2−Mn−O4	92.0(8)
<Mn−O>	1.99(2)	O3−Mn−O4	122.0(6)
Σradii	1.949	O2−Mn−O3	88.5(9)
Ho(1)−O1 (x3)	2.277(14)	O1−Mn−O4	86.4(7)
Ho(1)−O2 (x3)	2.293(8)	Mn−O3−Mn	118.3(9)
Ho(1)−O3	2.320(31)	Mn−O4−Mn	119.1(9)
Ho(2)−O1 (x3)	2.285(8)	Ho(1)−O1−Mn	127.8(9)
Ho(2)−O2 (x3)	2.297(11)	Ho(2)−O2−Mn	123.1(8)
Ho(2)−O4	2.437(21)		
<Ho(1)−O1,O2,O3>	2.29(4)		
<Ho(2)−O1,O2,O3>	2.31(4)		
Σradii	2.327		

Figure 8. View of the crystal structure of HoMnO₃, showing a layer of MnO₅ bipyramids sharing vertexes. Mn are the small dark spheres; O are the large spheres. The Ho³⁺ cations, lying between two adjacent layers, are not shown for the sake of clarity.

Figure 7. Observed (open circles) and calculated (solid line) neutron diffraction patterns at room temperature with $\lambda = 1.594$ Å. The Bragg reflections are drawn as tic marks, and the difference between the observed and calculated patterns is plotted at the bottom.

Figure 9. Thermal evolution of the NPD patterns, $\lambda = 2.42$ Å, showing the magnetic contribution to the scattering below T_N. Observe the sudden disappearance of the (101) magnetic reflection as a consequence of the spin reorientation.

propagation vector is $\mathbf{k} = 0$, the little group G_k coincides with the space group $P6_3cm$. According to Kovalev,[37] G_k has six irreducible representations, four, Γ_1, Γ_2, Γ_3, and Γ_4, that are unidimensional and two, Γ_5 and Γ_6, that are bidimensional. A Γ representation with the Fourier components of the magnetic moments, $\mathbf{m}_{ki}$, is constructed. The decomposition of Γ in terms of the irreducible representations of G_k are

for the Mn atoms,
$$\Gamma = \Gamma_1 + 2\Gamma_2 + 2\Gamma_3 + \Gamma_4 + 3\Gamma_5 + 3\Gamma_6$$
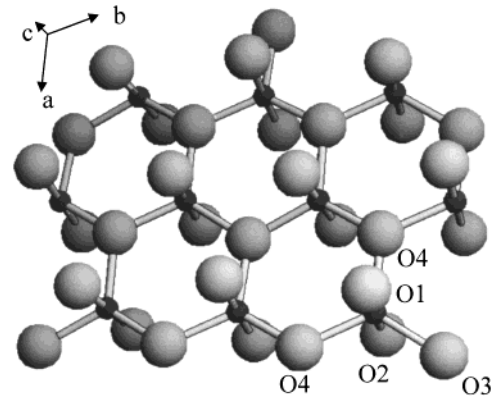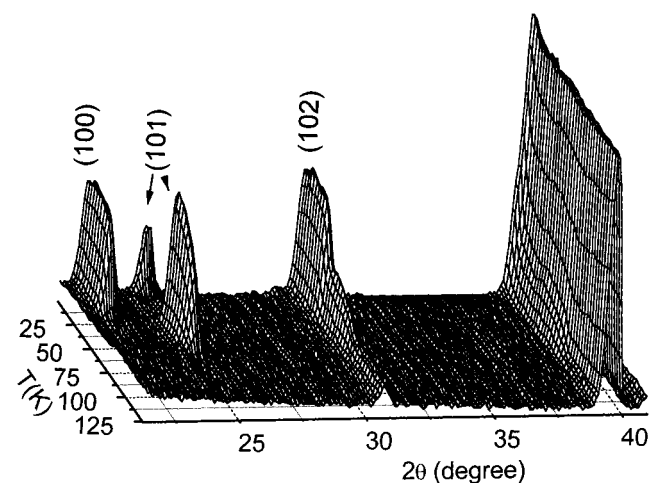
for the Ho(1) atoms (site 2a),
$$\Gamma = \Gamma_2 + \Gamma_3 + \Gamma_5 + \Gamma_6$$

for the Ho(2) atoms (site 4b),
$$\Gamma = \Gamma_1 + \Gamma_2 + \Gamma_3 + \Gamma_4 + 2\Gamma_5 + 2\Gamma_6$$

The basis vectors associated with each of the irreducible

representations were obtained by the operator projection method. The basis vectors corresponding to the Mn and Ho atoms are reported in Tables 3 and 4, respectively.

Below $T = 78.5$ K, after checking the different solutions described above, we obtain the best fit by assuming that only Mn spins are ordered and that they have the triangular structure given by the basis vectors corresponding to the irreducible representation Γ_2, with no component along the z direction. Thus, the magnetic moments lie parallel to the [100] axes, and the coupling
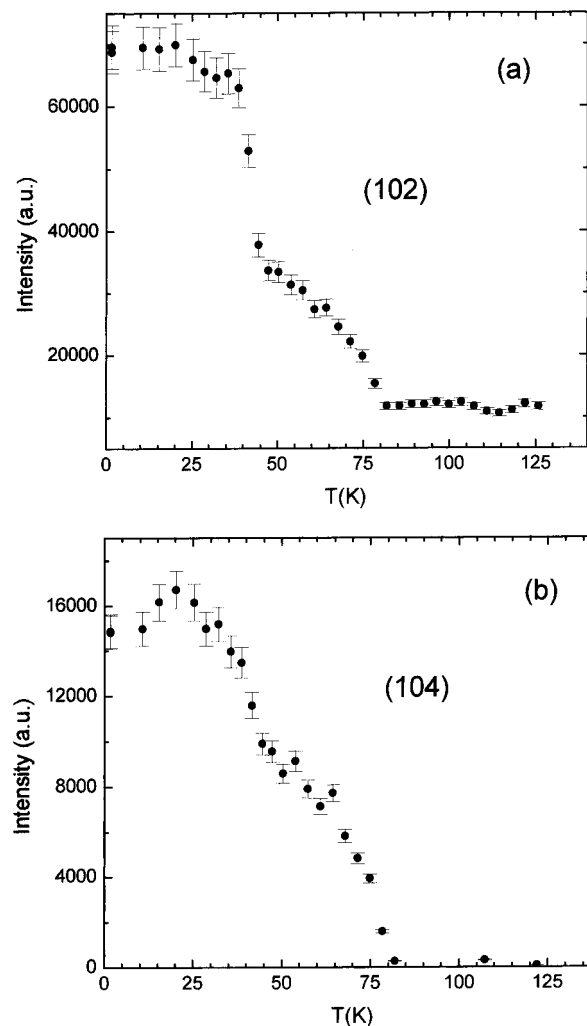
(37) Kovalev, O. V. *Representation of Crystallographic Space Groups*; Stokes, H. T., Hatch, D. M., Eds.; Gordon & Breach: Langhorne, PA, 1993.
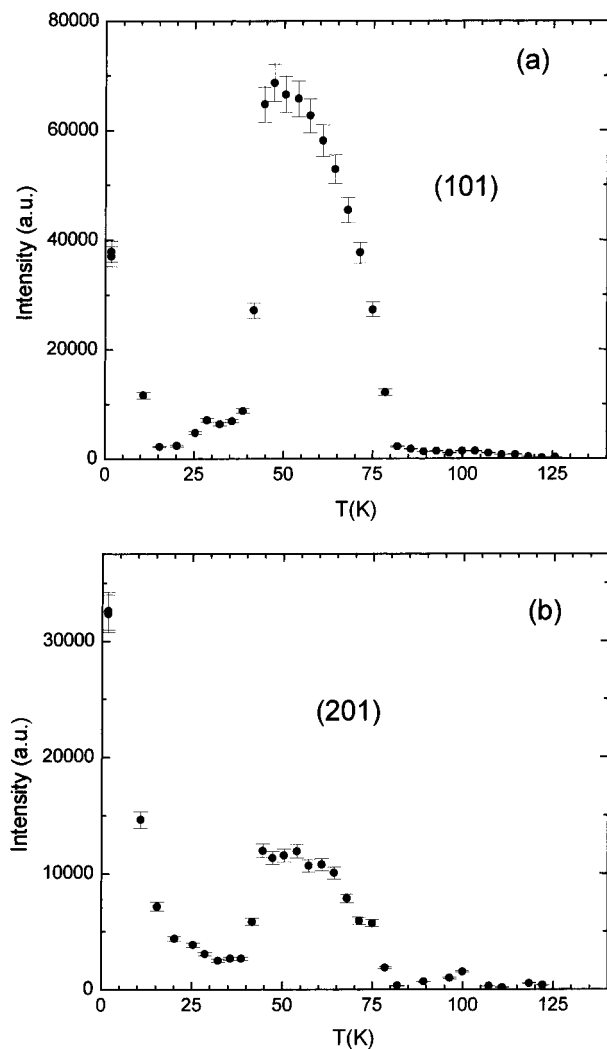
Figure 10. Integrated intensity vs temperature of some magnetic reflections: (a) (101) and (b) for (201).

Figure 11. Integrated intensity vs temperature of some magnetic reflections: (a) (102) and (b) for (104).

between the $z = 0$ and $z = {}^1/_2$ planes is AFM. As can be seen in Table 5, where the results of the fitting performed for the $T = 60.9$ K pattern are given, the magnetic moment for the Mn atoms is 2.52(2) μ_B at $T = 60.9$ K. The good agreement between the observed and calculated patterns is presented in Figure 13a. Below $T = 44.6$ K, the changes observed in the magnetic peaks can be explained by assuming that the moments suddenly rotate in the basal plane in such a way that, below $T = 38.8$ K, there are no further changes in the direction of the magnetic moments and the magnetic structure is defined by the irreducible representation Γ_1. Below this temperature, the Mn spins are perpendicular to the [100] axes. The thermal evolution of the magnetic moments and the angle with the $\mathbf{a_1}$ axis for Mn1, position $(x, 0, 0)$, are presented in Figure 14. At $T = 32.3$ K, the magnetic moment for the Mn atoms is 2.98(2) μ_B, and the observed and calculated patterns are compared in Figure 13b.

On the other hand, below $T = 25.4$ K, a better result in the fitting of the NPD patterns is obtained if a small moment is assumed to exist at the Ho(2) atom, site 4b. The magnetic moment of the Ho^{3+} cations rise as the temperature is decreased (see Figure 14), undergoing an appreciable increase especially below 15.5 K. The ordering of the Ho(2) atoms is given by the basis vector
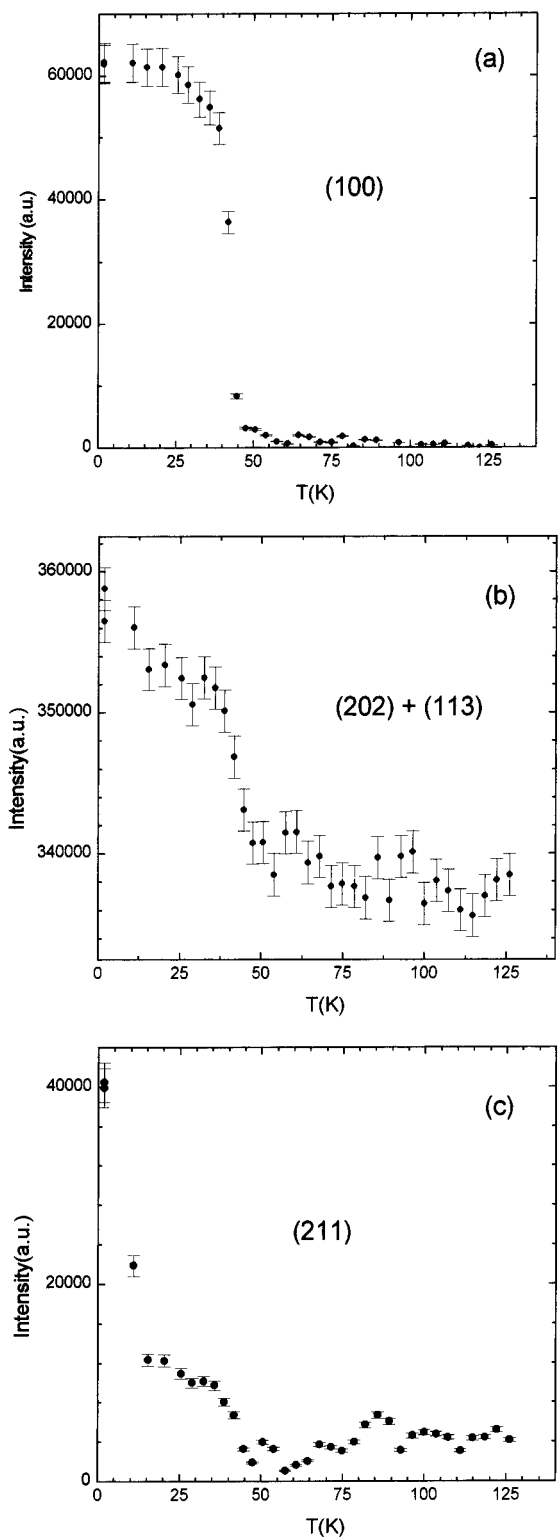
$(0, 0, A_z)$ associated with the Γ_1 representation. For $T = 1.7$ K, the magnetic moments are 3.05(2) and 2.87(3) μ_B for the Mn and Ho(2) atoms, respectively (see Table 3). The calculated and observed patterns at $T = 1.7$ K are illustrated in Figure 13c. A view of the different magnetic structures in each temperature interval is shown in Figure 15. The Ho(1) magnetic moments remain disordered, in a paramagnetic state, in all of the temperature ranges.

5. Discussion

The neutron diffraction results are in good agreement with the magnetic and specific-heat measurements. The sharp anomaly observed in the specific-heat curve at $T_N \approx 72$ K is related to the onset of the magnetic ordering of HoMnO$_3$, although initially only the Mn^{3+} ions are involved (they adopt a triangular spin arrangement in the basal plane). The transition observed at around 38 K corresponds to a reorientation of the magnetic moments of the Mn atoms in the basal plane. The anomaly detected in the specific-heat curve at around 4 K is related to the ordering of the Ho atoms, although neutron diffraction experiments have shown that they present a small ordered magnetic moment in the higher-temperature region. Although the ordering takes place at $T_N \approx 72$ K, the magnetic peaks are

Figure 12. Integrated intensity vs temperature of some magnetic reflections: (a) (100), (b) for (202) + (113), and (c) for (211).

Table 3. Basis Vector of the Mn Atoms that Occupies the 6c Site[a,b]

repr.	basis vector	Mn1 $(x, 0, 0)$	Mn2 $(0, x, 0)$	Mn3 $(-x, -x, 0)$	Mn4 $(-x, 0, \frac{1}{2})$	Mn5 $(0, x, \frac{1}{2})$	Mn6 $(x, x, \frac{1}{2})$
Γ_1	V_1^1	[120]	$[\bar{2}\bar{1}0]$	$[1\bar{1}0]$	$[\bar{1}\bar{2}0]$	[210]	$[\bar{1}10]$
Γ_2	V_1^2	[100]	[010]	$[\bar{1}\bar{1}0]$	$[\bar{1}00]$	$[0\bar{1}0]$	[110]
	V_2^2	[001]	[001]	[001]	[001]	[001]	[001]
Γ_3	V_1^3	[100]	[010]	$[\bar{1}\bar{1}0]$	[100]	[010]	$[\bar{1}\bar{1}0]$
	V_2^3	[001]	[001]	[001]	$[00\bar{1}]$	$[00\bar{1}]$	$[00\bar{1}]$
Γ_4	V_1^4	[120]	$[\bar{2}\bar{1}0]$	$[1\bar{1}0]$	[120]	$[\bar{2}\bar{1}0]$	$[1\bar{1}0]$
Γ_5	V_1^5	[100]	$\omega[0\bar{1}0]$	$\omega^*[110]$	[100]	$\omega[0\bar{1}0]$	$\omega^*[110]$
		$\omega^*[\bar{1}10]$	$\omega[0\bar{1}0]$	$[\bar{1}\bar{1}0]$	$\omega^*[\bar{1}00]$	$\omega[0\bar{1}0]$	$[\bar{1}\bar{1}0]$
	V_2^5	[010]	$\omega[110]$	$\omega^*[\bar{1}00]$	[010]	$\omega[110]$	$\omega^*[\bar{1}00]$
		$\omega^*[110]$	$\omega[\bar{1}00]$	[010]	$\omega^*[110]$	$\omega[\bar{1}10]$	[010]
	V_3^5	[001]	$\omega[00\bar{1}]$	$\omega^*[00\bar{1}]$	$[00\bar{1}]$	$\omega[001]$	$\omega^*[001]$
		$\omega^*[001]$	$\omega[00\bar{1}]$	[001]	$\omega^*[001]$	$\omega[001]$	$[00\bar{1}]$
Γ_6	V_1^6	[100]	$\omega[0\bar{1}0]$	$\omega^*[110]$	$[\bar{1}00]$	$\omega[010]$	$\omega^*[\bar{1}\bar{1}0]$
		$\omega^*[100]$	$\omega[0\bar{1}0]$	[110]	$\omega^*[\bar{1}00]$	$\omega[0\bar{1}0]$	$[\bar{1}\bar{1}0]$
	V_2^6	[010]	$\omega[110]$	$\omega^*[\bar{1}00]$	$[0\bar{1}0]$	$\omega[\bar{1}\bar{1}0]$	$\omega^*[100]$
		$\omega^*[\bar{1}\bar{1}0]$	$\omega[110]$	$[0\bar{1}0]$	$\omega^*[110]$	$\omega[\bar{1}00]$	[010]
	V_3^6	[001]	$\omega[00\bar{1}]$	$\omega^*[00\bar{1}]$	[001]	$\omega[00\bar{1}]$	$\omega^*[00\bar{1}]$
		$\omega^*[001]$	$\omega[00\bar{1}]$	[001]	$\omega^*[001]$	$\omega[001]$	$[00\bar{1}]$

[a] The directions are denoted by $[e_x e_y e_z]$, where e_x and e_y are in the basal plane forming an angle of 120° between them and e_z is parallel to the 6-fold axis. [b] $\omega = e^{i\pi/3}$.

Table 4. Basis Vectors of the Ho(1) and Ho(2) Atoms that Occupy, Respectively, the 2a and 4b Sites[a]

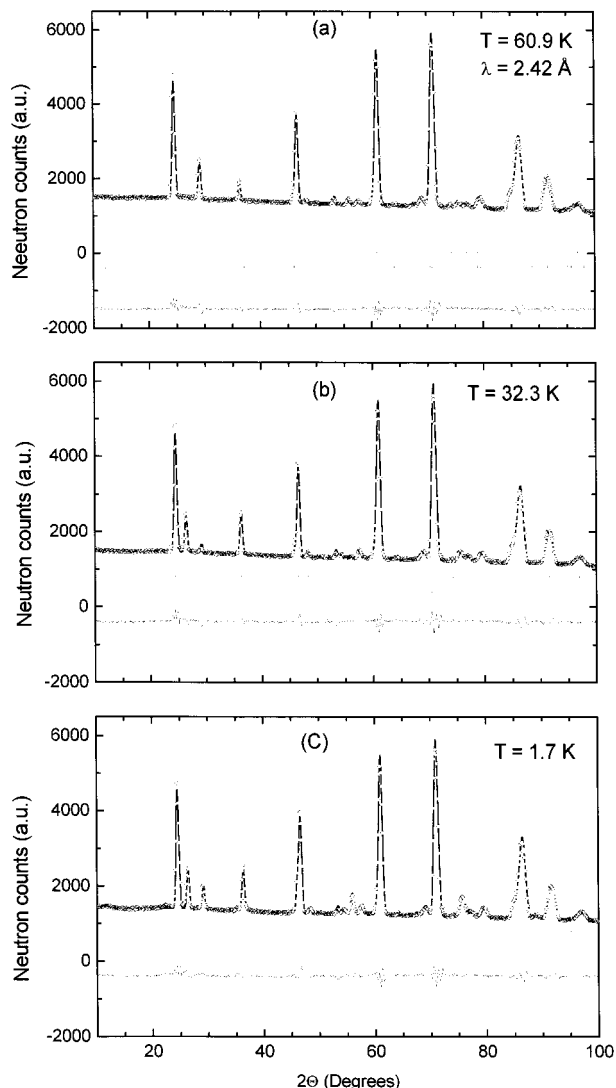| repr.	basis vector	Ho(1) 2a Ho1 $\begin{pmatrix}0\\0\\z\end{pmatrix}$	Ho2 $\begin{pmatrix}0\\0\\z+\frac{1}{2}\end{pmatrix}$	Ho3 $\begin{pmatrix}\frac{1}{3}\\\frac{2}{3}\\z\end{pmatrix}$	Ho(2) 4b Ho4 $\begin{pmatrix}\frac{2}{3}\\\frac{1}{3}\\z\end{pmatrix}$	Ho5 $\begin{pmatrix}\frac{1}{3}\\\frac{2}{3}\\z+\frac{1}{2}\end{pmatrix}$	Ho6 $\begin{pmatrix}\frac{2}{3}\\\frac{1}{3}\\z+\frac{1}{2}\end{pmatrix}$
Γ_1	V_1^1	−	−	[001]	$[00\bar{1}]$	$[00\bar{1}]$	[001]
Γ_2	V_1^2	[001]	[001]	[001]	[001]	[001]	[001]
Γ_3	V_1^3	[001]	$[00\bar{1}]$	[001]	[001]	$[00\bar{1}]$	$[00\bar{1}]$
Γ_4	V_1^4	−	−	[001]	$[00\bar{1}]$	[001]	$[00\bar{1}]$
Γ_5	V_1^5	[uv0]	[uv0]	[pq0]	[rs0]	[rs0]	[pq0]
Γ_6	V_1^6	[uv0]	$[\bar{u}v0]$	[pq0]	[rs0]	$[\bar{r}s0]$	$[\bar{p}\bar{q}0]$

[a] The directions are denoted by $[e_x e_y e_z]$, where e_x and e_y are in the basal plane forming an angle of 120° between them and e_z is parallel to the 6-fold axis.

patterns would be indistinguishable if the moments were rotated by 90° in the basal plane and the coupling between the $z = 0$ and $z = \frac{1}{2}$ layers were changed in sign (from AFM to FM and vice versa). That is to say, the magnetic modes Γ_2 and Γ_4 would be indistinguishable, as well as the modes Γ_1 and Γ_3, if the atomic positions for the Mn atoms were $x \approx \frac{1}{3}$. In our case, $x = 0.322(3)$ for HoMnO₃; given the good quality of our neutron data, this difference with respect to $\frac{1}{3}$ is enough for a significant difference to be observed between the agreement factors for Γ_2 and Γ_1 (AFM coupling of the layers) versus Γ_4 and Γ_3 (ferromagnetic coupling of the layers).

If we consider the magnetic structures associated with Γ_4 and Γ_3, we obtain discrepancy factors, R_{mag}, of 9.6% at $T = 60.9$ K (with Γ_4) and 13.8% at $T = 60.9$ K (with Γ_3). Below 25.4 K, the ordering of the Ho atoms must be included. Considering that the spin arrangement for the Mn atoms is given by Γ_3, the ordering of the Ho atoms must also be defined by this representation, giving rise to a very different magnetic arrangement from that reported in Table 3. In this case, for Γ_3, both the Ho(1) and Ho(2) atoms would be ordered with the

present below 78.5 K; this small discrepancy could be due to calibration problems, or it could be related to the different heating regimes and the different amounts of sample studied during magnetic (50 mg) and neutron (4 g) data collection.

As was pointed out by Bertaut et al.,[21] for a perfect triangular spin arrangement in the basal plane of the hexagonal RMnO₃ compounds, the neutron diffraction

Table 5. Mean Results Obtained in the Fitting of the Magnetic Structure in the Different Temperature Domains

	$T = 60.9$ K			$T = 32.3$ K			$T = 1.7$ K		
	Mn	Ho(1)	Ho(2)	Mn	Ho(1)	Ho(2)	Mn	Ho(1)	Ho(2)
mom. (μ_B)	2.52(2)	–	–	2.98(2)	–	–	3.05(2)	–	2.87(3)
solution	Γ_2			Γ_1			Γ_1		Γ_1
discrep.	R_{Bragg} (%)		3.4			3.7			4.0
factors	R_{Magn} (%)		9.3			10.0			7.5
	χ^2		2.1			2.4			1.1

Figure 13. Observed (open circles) and calculated (solid line) NPD patterns in the ordering region with $\lambda = 2.42$ Å. The two series of tic marks correspond to the nuclear Bragg reflections and the magnetic peaks. The difference pattern is plotted at the bottom. (a) $T = 60.9$ K, (b) $T = 32.3$ K, and (c) $T = 1.7$ K.

moments lying along the z direction. The magnetic moment would differ for the two sites, being $m_{Ho(1)} = 3.85(10)$ μ_B and $m_{Ho(2)} = -1.33(10)$ μ_B at $T = 1.7$ K. The two atoms that occupy the 2a site, Ho(1), would be antiferromagnetically coupled, whereas the arrangement of the Ho moments at the 4b site is defined by (0, 0, C_z). At this temperature, $T = 1.7$ K, we obtain a discrepancy factor $R_{mag} = 11.1\%$, again significantly worse than that corresponding to Γ_1, which is 7.5% (Table 3). Our results suggest that the magnetic structures of hexagonal HoMnO$_3$ are defined by Γ_2 (above the spin-reorientation temperature) and by Γ_1 (below the spin-reorientation temperature), even though this
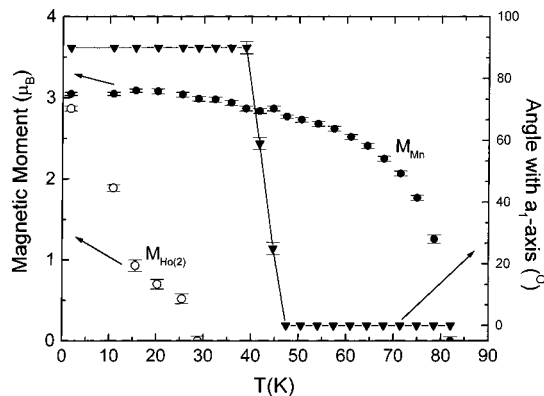
Figure 14. Thermal evolution of the magnetic moments for Mn and Ho(2) atoms.
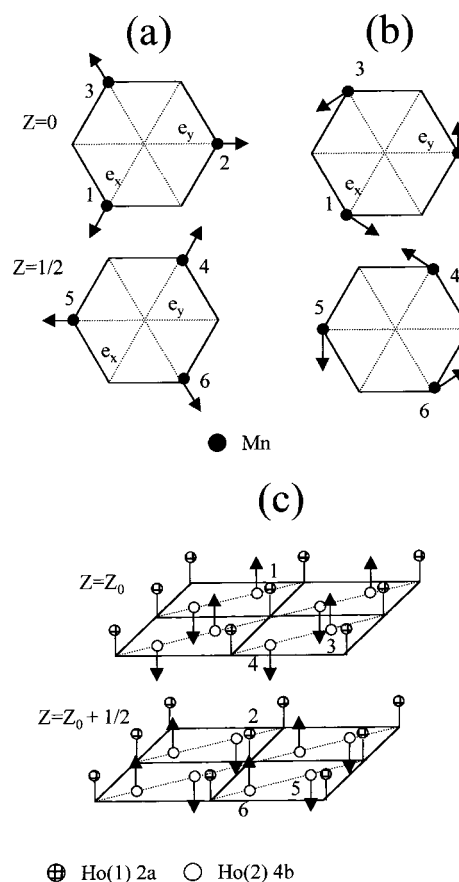
Figure 15. Scheme of the magnetic structure of HoMnO$_3$: (a) $44.6 < T < 78.5$ K, (b) $25.4 < T < 44.6$ K, and (c) $T < 25.4$ K. Note: For $T < 25.4$ K, the Mn atoms are ordered according to the magnetic structure given in panel b.

is in disagreement with a recent study carried out with the second harmonic spectroscopy technique,[27] which seems to indicate that the coupling between the $z = 0$ and $z = \frac{1}{2}$ layers is FM and that, hence, the magnetic ordering would be represented by Γ_4 and Γ_3. As further

support for our results, we must mention that ScMnO$_3$, which shows the same magnetic arrangement,[29] exhibits weak ferromagnetism at low temperatures, which is only compatible with the Γ_2 solution and, therefore, with an AFM coupling of the layers, despite the fact that the second harmonic spectroscopy technique[27] also suggested a FM coupling for this compound.

The magnetic moment of the Mn^{3+} ions at $T = 1.73$ K is 3.05 μ_B. This implies that the ground state of the Mn^{3+} ions is in the high-spin configuration. The level scheme of the d^4 orbitals in a bipyramidal configuration can be deduced, as in YMnO$_3$.[38,39] In the paraelectric state at high temperature, the space group is $P6_3/mmc$, and the $\bar{6}m2$ point symmetry of the MnO$_5$ bipyramid splits the d^4 orbitals into a singlet plus two doublets. In the low-temperature ferroelectric state, the symmetry is $P6_3cm$, and the point symmetry of the bipyramid decreases to m, which originates the splitting of each doublet into two singlets. The d^4 electrons would occupy four singlets, and the strong hybridization of the last-occupied singlet with the 2p oxygen orbital would give rise to a magnetic moment magnitude below 4 μ_B.

The paramagnetic temperature, $\theta_P = -17$ K, implies that the magnetic exchange interactions are predominantly AFM. This is confirmed by the magnetic structure found from neutron diffraction experiments. The Mn^{3+} ions interact via superexchange interactions through Mn$-$O$-$Mn bonds. In the basal plane, the two exchange paths are Mn$-$O3$-$Mn and Mn$-$O4$-$Mn. However, the Mn^{3+} ions are arranged in a perfect triangular net, with the O^{2-} ions (O3 and O4) at the center of each triangle. The three Mn^{3+} ions interact via the same O^{2-} ion, and the impossibility of all of them being antiferromagnetically coupled provides the driving force for the triangular magnetic structure observed in the basal plane. The Mn$-$O3$-$Mn and Mn$-$O4$-$Mn bond angles are close to 120°; therefore, the interaction between filled e$_g$ states can take place via the same oxygen p orbital as well as via two perpendicular p orbitals. According to the Goodenough rules,[40] the superexchange interaction involves both AFM and FM interactions; both types of interactions are present in the triangular spin arrangement, although the AFM coupling seems to predominate. The orientation of the

moments in the *ab* plane is determined by second-order relativistic terms.

Our results suggest that direct Ho$-$Ho exchange interactions are responsible for the Ho magnetic ordering, because the Ho atoms order at relatively low temperature and, as well, because of symmetry considerations. Each of the atoms Ho(1) and Ho(2) is at the top of a pyramid whose basis is formed by an equilateral triangle with the Mn atoms at the apexes. As the three Mn atoms have a triangular spin arrangement, the total magnetic moment is zero, and therefore, according to the classical Weiss molecular field approximation, the magnetic moment induced by the Mn atoms at the Ho sites is zero. With respect to the Ho$-$Ho exchange interactions, on one hand, Ho(1) atoms have six Ho(2) atoms as nearest neighbors, which are at a distance of 3.578 Å (the 2a site is placed at the 6-fold axis); on the other hand, for the Ho(2) atoms, the nearest neighbors are three Ho(2) and three Ho(1) atoms localized at distances of 3.546 and 3.579 Å, respectively. Considering the magnetic structure defined by Γ_1, the six nearest-neighbor Ho(2) atoms are divided into two groups of three atoms that are antiferromagnetically coupled between them (see Figure 15). According to the classical Weiss molecular field approximation, the induced magnetic moment at the Ho(1) site is zero, which would explain why these atoms remain in a paramagnetic state down to 1.7 K.

6. Conclusion

The magnetic properties and magnetic structure of HoMnO$_3$ have been revisited. Magnetization and specific-heat measurements show that HoMnO$_3$ becomes ordered at $T_N \approx 72$ K, and that below this temperature, another two magnetic transitions take place. Neutron diffraction measurements confirm that the Mn magnetic moments order according to a triangular spin arrangement. At around $T = 44.6$ K, the moments reorientate in the basal plane in such a way that they become placed perpendicularly with respect to the initial direction. The best fit is achieved for a model in which the coupling between the $z = 0$ and $z = \frac{1}{2}$ layers is antiferromagnetic. Below $T = 25.4$ K, a magnetic moment is observed at the Ho(2) atoms at 4b sites; the Ho(1) moments remain in the paramagnetic state down to 1.7 K.

(38) Frölich, D.; Leute, St.; Pavlov, V. V.; Pisarev, R. V. *Phys. Rev. Lett.* **1998**, *81*, 3239.

(39) Medvedeva, J. E.; Anisimov, V. I.; Korotin, M. A.; Myrasov, O. N.; Freeman, A. J. *J. Phys. Condens. Matter* **2000**, *12*, 4947.

(40) Goodenough, J. B. *Magnetism and the Chemical Bond*; Interscience Publishers: New York, 1963.